11-2012

Modeling and simulation of pressure waves generated by nano-thermite reactions

Karen S. Martirosyan
The University of Texas Rio Grande Valley

Maxim Zyskin
Rutgers University - New Brunswick/Piscataway

Charles M. Jenkins
Eglin AFB

Yasuyuki Horie
Eglin AFB

Modeling and simulation of pressure waves generated by nano-thermite reactions

Karen S. Martirosyan,[1,a)] Maxim Zyskin,[2] Charles M. Jenkins,[3] and Yasuyuki (Yuki) Horie[3]
[1]*Department of Physics and Astronomy, University of Texas, Brownsville, 80 Fort Brown, Brownsville, Texas 78520, USA*
[2]*Rutgers University, 126 Frelinghuysen Road, Piscataway, New Jersey 08854-8019, USA*
[3]*Air Force Research Lab, Munitions Directorate, 2306 Perimeter Road, Eglin AFB, Florida 32542, USA*

(Received 8 August 2012; accepted 9 October 2012; published online 8 November 2012)

This paper reports the modeling of pressure waves from the explosive reaction of nano-thermites consisting of mixtures of nanosized aluminum and oxidizer granules. Such nanostructured thermites have higher energy density (up to 26 kJ/cm^3) and can generate a transient pressure pulse four times larger than that from trinitrotoluene (TNT) based on volume equivalence. A plausible explanation for the high pressure generation is that the reaction times are much shorter than the time for a shock wave to propagate away from the reagents region so that all the reaction energy is dumped into the gaseous products almost instantaneously and thereby a strong shock wave is generated. The goal of the modeling is to characterize the gas dynamic behavior for thermite reactions in a cylindrical reaction chamber and to model the experimentally measured pressure histories. To simplify the details of the initial stage of the explosive reaction, it is assumed that the reaction generates a one dimensional shock wave into an air-filled cylinder and propagates down the tube in a self-similar mode. Experimental data for Al/Bi_2O_3 mixtures were used to validate the model with attention focused on the ratio of specific heats and the drag coefficient. Model predictions are in good agreement with the measured pressure histories. © *2012 American Institute of Physics*. [http://dx.doi.org/10.1063/1.4764319]

I. INTRODUCTION

Nanostructured highly exothermic reactive mixtures, referred to as nanoenergetic materials (NM) or metastable intermolecular composites (MIC), may release energy much greater than conventional energetic materials.[1–3] A comparison of energy densities of monomolecular energetic materials with NM shows that the volumetric energy of NM can easily exceed the best existing molecular explosives by about a factor of two and can have values up to 26 kJ/cm^3.[4] However, due to the granular nature of thermite energetic materials, reaction kinetics is typically controlled by the mass transport rates on the reactants surfaces. Hence, although thermite composites may have extreme energy densities, the release rate of that energy is below that which may be attained in a chemical kinetics controlled process. To reduce the diffusion limitation and associated mass transport in the thermite composites the attempt was made to use nanostructured components.[5–9] Based on these developments, the research on nanostructured energetic materials is getting more attention and interest from many research groups worldwide. Nano-scale particles have a significantly higher surface area to volume ratio than micro-particles, providing a closer contact between solid particles in energetic mixtures. The small size of nano-particles increases the homogeneity of the reactant mixture and improves the uniformity of a propagating reaction front.

Recent studies revealed that aluminum-oxidizer nanocomposites, such as Al/Bi_2O_3 nano mixtures, can generate a transient pressure pulse up to seven times larger than that during the explosion of traditional thermite reactive mixtures. Moreover, the combustion of such nano mixtures demonstrated four times higher gas release than molecular explosives such as conventional trinitrotoluene (TNT). A possible explanation for the high pressure rise during the combustion of Al/Bi_2O_3 nanosystems is that the reaction time in such nanosystems is much smaller than time for a gas shock wave to leave the reaction region, so in effect all the energy is released into gas almost instantaneously. A solution of equations of gas dynamics indicates that a large shock wave pressure jump will occur in such case. Bismuth, one of the reaction products, boils at a temperature of 1560 °C, which is lower than the maximum reaction temperature 2700 °C. This causes quick bismuth evaporation and provides a mechanism of quick transfer of energy into gas.

The shock wave velocity and rate of energy release increased by up to 3 orders of magnitude when the particles size of either aluminum and/or the oxidizer were reduced to a nanosize range.[10,11] A pressure discharge up to 11 MPa was generated by using Al/Bi_2O_3 nanosystems (with sample mass 0.5 g and chamber volume 0.342 L) are shown in Figure 1.[11] A very large (several orders of magnitude) difference existed between the rate of the pressure pulse release by nanothermite reactions and by thermite reactions with large aluminum particles. The maximum observed pressurization rate was 3200 GPa/s. The time needed to reach the peak pressure was 0.01 ms for aluminum particles with diameter of 100 nm.[3,4]

The characteristic features of the Al/Bi_2O_3-based nanothermite mixtures indicate potential for applications as propulsion, explosives, and pyrotechnic components. Thus, nanostructured energetic materials are a subject of increased

a)Electronic mail: karen.martirosyan@utb.edu.

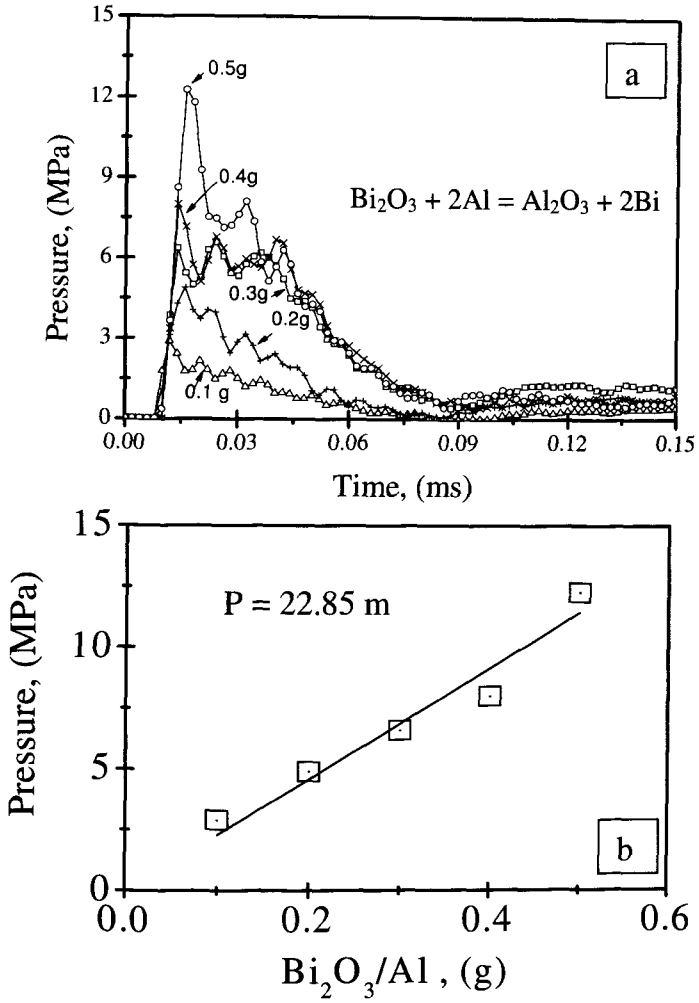

FIG. 1. (a) Typical experimental temporal pressure discharge during the $Bi_2O_3 + 2Al = Al_2O_3 + 2Bi$ nano-thermite reaction. The combustion was conducted inside a commercial "Parr" stainless steel cylindrical reactor with radius 30.7 mm and length 115 mm (V = 0.342 L). High-frequency pressure transducer (PCB Piezotronics Inc.) was placed on top of the reactor. A nano-energetic mixture (0.5 g) was loaded into a ceramic boat, placed into the reactor. The reactants mixture was ignited by an electrically heated coil, inserted into the sample. The pressure transducer was recorded and processed by an Omega data acquisition board connected to a PC with a resolution of 1 microsecond. (b) Peak pressure dependence on mass of Al/Bi_2O_3 mixture.

interest for many applications since they have improved properties compared with their micro- or macroscopic counterparts. High density nanoenergetic materials have various potential emerging applications and are likely to become the next-generation explosive and propulsion materials. They enable adjustment of the energy density and power release by tuning of composite stoichiometry, control of the particle shape, size distribution, porosity, and density. A complete balance between the oxidizer and fuel may be reached to maximize energy density. The development of novel nanoenergetic materials, their design, synthesis, and fabrication procedures are critical for national security, and they have been recognized as a significant addition to the support of changing force structure for advanced weapons platforms. While several new promising concepts and formulations[3–8] have emerged in recent years, the Department of Defense is continuing to support the ability to maintain and improve the knowledge base in this area.

Since a simple explanation of higher pressure generation is not addressed by the equation of state determined using micron or sub-micron materials, further experimental research and analysis of pressure generation is needed at the nano level. During the explosion, various physical processes such as thermal heating and expansion, vaporization, complex gas, and particles motions behind shock waves can occur. The theory of explosions includes two main topics: (a) the propagation of blast waves in unbounded media; (b) the interaction of blast waves with different obstacles and shocks. The goal of this paper is to model and predict the pressurization behavior of explosion of nanoenergetic materials by using equations of gas dynamics. The experimental data were used for the illustration of the theoretical conclusions.

A. Formulation of the problem

A stainless steel cylindrical reactor with radius 30.7 mm and length 115 mm (volume V = 0.342 L) was used to measure pressure discharge at the top of the reactor. This high pressure reactor was used to obtain experimental data shown in Figure 1, published recently in Ref. 11. We assume that an explosion happens at the closed end of a cylinder with the cross-section area S and that the pressure observation occurs at a distance L away from the explosion. We assume that a one dimensional explosion occurs in the direction of the axes of a cylindrical tube and that explosion is uniform in the cross-section of the tube, as illustrated in Figure 2. Our actual reactor geometry is favorable for such an explosion to occur. We assume that the explosion is very quick and all the explosion energy is released into the gas instantaneously in a thin cross-section of the cylinder. We also assume that the pressure in the shock wave which forms after the explosion is much greater than the pressure of the ambient gas (strong explosion). An explicit self-similar solution for a strong instantaneous explosion was first obtained in the spherical symmetric case by Neumann[12] and by Taylor[13] and for the spherical, plane, and cylindrical case by Sedov.[14] Detailed analysis of a self-similar solution reveals that if the gas pressure as well as the contribution of the drag force per unit area are taken into account, a good match with nanothermite mixtures experiments is achieved.

Not all explosions can be described by such a self-similar solution; for example, if energy is released more slowly, we expect a more washed-out solution with a smaller shock wave pressure. But a self-similar solution is expected to give a good model for very strong and quick explosions (in fact such solutions were compared with nuclear explosions[13]). A good match of nanothermite mixtures experiments with a self-similar solution indicates that nanothermite mixtures are very efficient in creating high shock wave pressures.

II. GAS DYNAMICS MODELING

A. Shock adiabate in polytropic gas

We consider here gas dynamics in one spatial dimension (along the axis of a cylindrical reactor). For adiabatic flow, equations of gas dynamics can be presented as the conservation of momentum, entropy, and mass

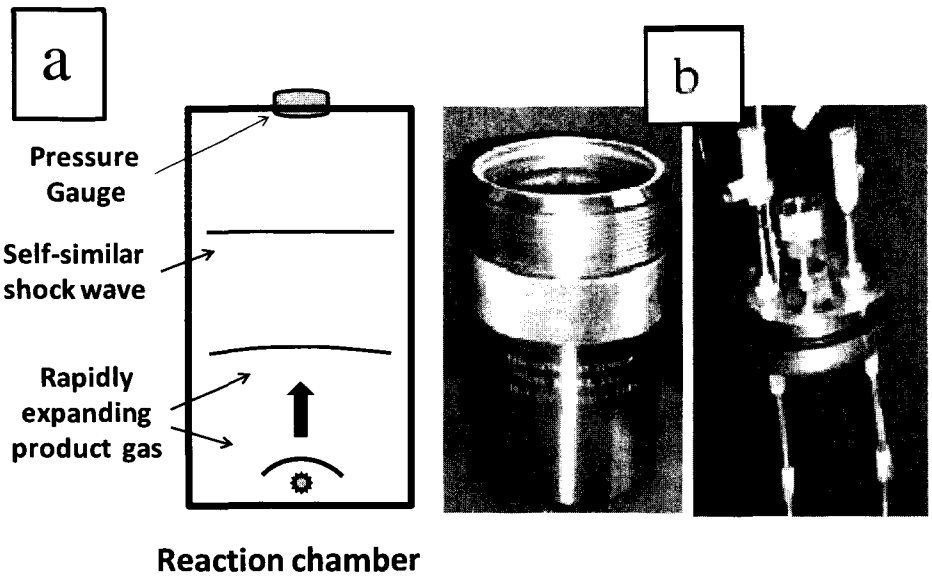

FIG. 2. (a) Schematic diagram of cylindrical reactor, which shows as the thin layer of shock wave propagated upward direction. (b) Experimental setup for measuring gas pressure discharge.

$$\begin{aligned}\frac{\partial}{\partial t}(\rho v) &= -\frac{\partial}{\partial x}(\rho v^2 + P),\\ \left(\frac{\partial}{\partial t} + v\frac{\partial}{\partial x}\right)s &= 0,\\ \frac{\partial \rho}{\partial t} + \frac{\partial(\rho v)}{\partial x} &= 0,\end{aligned} \tag{1}$$

here x is the coordinate along the axis of the cylinder, t time, $\rho = \rho(x,t)$ gas density, $v = v(x,t)$ gas velocity at (x,t), $P = P(x,t)$ gas pressure, $s = s(x,t)$ gas entropy per unit mass, and $\varepsilon = \varepsilon(x,t)$ gas energy per unit mass. We note that the second equation in Eq. (1), the conservation of entropy may be replaced by the conservation energy

$$\frac{\partial\left(\rho\left(\varepsilon + \frac{v^2}{2}\right)\right)}{\partial t} = -\frac{\partial\left(\rho v\left(\varepsilon + \frac{P}{\rho} + \frac{v^2}{2}\right)\right)}{\partial x}. \tag{2}$$

The resulting system of equations is equivalent to Eq. (1). We further discuss equivalent formulations of Eq. (1) in the Appendix.

At a shock wave discontinuity moving with a velocity $u = u(t)$, the boundary conditions follow from the conservation of mass, momentum, and energy. Those are easiest to derive in a reference system moving with the shock wave, as it is done in Ref. 15. In the laboratory reference system, those boundary conditions may be written as

$$\begin{aligned}[\rho(v-u)] &= 0,\\ [P + \rho(v-u)^2] &= 0,\\ \left[\frac{1}{2}(v-u)^2 + \varepsilon + \frac{P}{\rho}\right] &= 0.\end{aligned} \tag{3}$$

here the square brackets $[\ldots]$ denote shock wave jump discontinuity, u is the velocity of the shock wave, and v is gas velocity; all velocities are expressed in the laboratory system of reference. Below we will denote quantities ahead of the shock wave by subscript 1 and those behind the shock wave by 2, so that ρ_1, v_1, P_1 is density, velocity, pressure in front of the shock wave and ρ_2, v_2, P_2 is density, velocity, pressure behind the shock wave. Derivation of conditions (3) is standard and is easiest in a system of reference moving with the shock wave.[15]

Jump conditions at a shock wave discontinuity (3) lead to the Rankine-Hugoniot shock adiabate relation

$$\varepsilon_1 - \varepsilon_2 + \frac{1}{2}\left(\rho_1^{-1} - \rho_2^{-1}\right)(P_1 + P_2) = 0. \tag{4}$$

For a polytropic gas with a constant adiabatic index $\gamma = \frac{c_p}{c_v}$, where c_p is heat capacity per unit mass at constant pressure and c_v heat capacity per unit mass at constant volume, we have that $\varepsilon = \frac{1}{\gamma - 1}\frac{P}{\rho}$, and solving Eq. (4) for $\frac{\rho_2}{\rho_1}$ yields

$$\frac{\rho_2}{\rho_1} = \frac{(\gamma-1)P_1 + (\gamma+1)P_2}{(\gamma+1)P_1 + (\gamma-1)P_2}. \tag{5}$$

If the pressure behind the shock wave is much greater than in front of it, $P_2 \gg P_1$, it follows from Eq. (5) that

$$\frac{\rho_2}{\rho_1} = \frac{\gamma+1}{\gamma-1}. \tag{6}$$

Since the mass conservation requires $\rho_2(v_2 - u) = -\rho_1 u$ and using Eq. (6) for $\frac{\rho_1}{\rho_2}$, it follows that

$$v_2 = \frac{2}{\gamma+1}u, \tag{7}$$

which, in particular, means that the gas behind is moving slower than the shock wave itself. From the momentum conservation (the second equation in Eq. (3)), we have that $P_2 + \rho_2(v_2 - u)^2 = P_1 + \rho_1 u^2$, and in the case $P_2 \gg P_1$ we can disregard P_1 and use Eqs. (6) and (7) to get

$$P_2 = \rho_1 u^2 - \rho_2(v_2 - u)^2 = \frac{2}{\gamma+1}\rho_1 u^2. \tag{8}$$

Strong shock discontinuity relations (6)–(8) give rise to the boundary conditions (A3) for the self-similar solution, described in detail in the Appendix; in particular, they allow for the computation of the total force per unit area measured by the detector right at the arrival time of the shock wave (14).

B. Big explosion model: A self-similar solution of gas dynamics

The main assumptions of the big explosion model are that (a) explosion occurs very quickly, so that all the explosion energy E is released before a shock wave leaves a very narrow explosion region and (b) the pressure behind the shock wave is much larger than pressure of the gas into which it is expanding (and so strong discontinuity conditions (6)–(8) can be used). We assume that an explosion happens at an end of a cylinder with a cross-section S and length L; and the pressure observation is made a distance L away from the explosion. The test geometry suggests that the solution is one dimensional, depending only on the coordinate along the cylinder axes and uniform in a cross-section of a cylinder. We seek a self-similar solution of the gas dynamics equations, propagating along the axes of a cylindrical reactor and exhibiting a shock wave. We will compare such a self-similar solution with the experiments. Results of comparison show a very good match.

By dimensional considerations, we shall seek a solution with the position of the shock discontinuity at time t given by

$$X = \beta\left(\frac{Et^2}{S\rho_1}\right)^{\frac{1}{3}}, \tag{9}$$

here $X = X(t)$ is the shock wave position, E energy released in the explosion, S reactor cross-section, ρ_1 is the gas density in front of the shock wave, and β is a dimensionless constant. Indeed, we assume a uniform distribution in the cylinder cross-section, so only the energy per unit cross sectional area $\frac{E}{S}$ can appear; the only combination of quantities E, S, ρ_1, t with the dimension of length is the one given in Eq. (9). The unknown dimensionless constant β is to be determined in the process of solution (see Eq. (A18)). The velocity of the shock wave is then

$$u = \frac{dX}{dt} = \frac{2X}{3t} = \frac{2\beta}{3}\left(\frac{E}{S\rho_1 t}\right)^{\frac{1}{3}}, \tag{10}$$

and the pressure right behind the shock wave is given by Eq. (8)

$$P_2 = \frac{8\beta^2\rho_1}{9(\gamma+1)}\left(\frac{E}{S\rho_1 t}\right)^{\frac{2}{3}}. \tag{11}$$

It follows from Eq. (10) that the shock wave will travel the distance L to the detector in time t_* given by

$$t_* = \left(\frac{\rho_1 L^3 S}{\beta^3 E}\right)^{\frac{1}{2}}. \tag{12}$$

Using Eq. (11) for the pressure, together with Eq. (12) for the shock wave arrival time, the pressure P_* just behind the shock at the time of arrival to the detector is

$$P_* = \frac{8\beta^3}{9(\gamma+1)}\left(\frac{E}{V}\right), \tag{13}$$

where $V = S\,L$ is the chamber volume (the volume which explosion fills before reaching the detector).

In fact, a detector will measure not just the incoming pressure, but a combination of the incoming gas pressure and drag force of the incoming flow per unit area; at a time t greater than the shock arrival time t_* this is given by $P + \frac{1}{2}\alpha\rho v^2$, where α is the drag coefficient. We expect that $\alpha = 0$ if a detector is parallel to the flow and does not feel the drag, and $\alpha = 2$ if a detector is perpendicular to the flow. A detector perpendicular to the flow is a blunt body, and bluff bodies typically have drag coefficients in the range from 1 to slightly above 2; in particular, a long plate perpendicular to a flow has $\alpha = 2$. Our test geometry suggests that the flow is strongly disrupted by the detector as the flow cannot easily go around it, and using $\alpha = 2$ is appropriate ($\alpha = 2$ corresponds to the case where all the incoming flow momenta passing through the detector cross-section is transferred to the detector, which is indeed expected to happen in our test geometry). Further discussion of drag coefficients can be found in Refs. 16–18.

Right at the arrival time t_* of the shock wave to the detector, the pressure + drag contribution follows immediately from the strong shock discontinuity conditions (6)–(8), and the result for the velocity of the shock wave (10). Indeed, $v_*^2 = \left(\frac{2}{\gamma+1}\right)^2 u^2$, $\rho_* = \frac{\gamma+1}{\gamma-1}\rho_1$, and

$$\left(P + \frac{1}{2}\alpha\rho v^2\right)_* = P_* + \frac{1}{2}\alpha\rho_* v_*^2 = \frac{8\beta^3}{9(\gamma+1)}\left(\frac{E}{V}\right)\left(1 + \frac{\alpha}{\gamma-1}\right). \tag{14}$$

here we denote by $*$ the quantities right at the arrival of the shock wave.

At times past the arrival time of the shock wave, where the pressure + drag contribution is $P + \frac{1}{2}\alpha\rho v^2$, we need to solve the gas dynamic equation (1) in order to determine P, ρ, v. If the explosion happens very quickly with all the energy released instantaneously, the solution is well approximated by a self-similar solution, which depends on a dimensionless variable $\xi = \frac{x}{X}$, where X is given by Eq. (9), and velocity, density, and pressure v, ρ, P can be found from equations for their dimensionless counterparts $\mathcal{V}, \mathcal{D}, \mathcal{Z}$

$$v = \frac{2x}{3t}\mathcal{V}(\xi), \quad \rho = \rho_1\mathcal{D}(\xi), \quad P = \frac{1}{\gamma}\left(\frac{2x}{3t}\right)^2\rho_1\mathcal{D}(\xi)\mathcal{Z}(\xi). \tag{15}$$

Substituting such an anzats into the gas dynamic equation (1) yields a system of ordinary differential equations (ODE) for dimensionless functions $\mathcal{V}(\xi), \mathcal{D}(\xi), \mathcal{Z}(\xi)$. This system of ODE, together with the strong discontinuity conditions (6)–(8), admits an explicit solution (first discovered in the spherical case by Neumann[12] and by Taylor,[13] and in plane and cylindrical case by Sedov[14]). We give details of a derivation of the self-similar solution in the Appendix. In particular, $\mathcal{V}(\xi)$ is the function inverse to the function $\xi(V)$

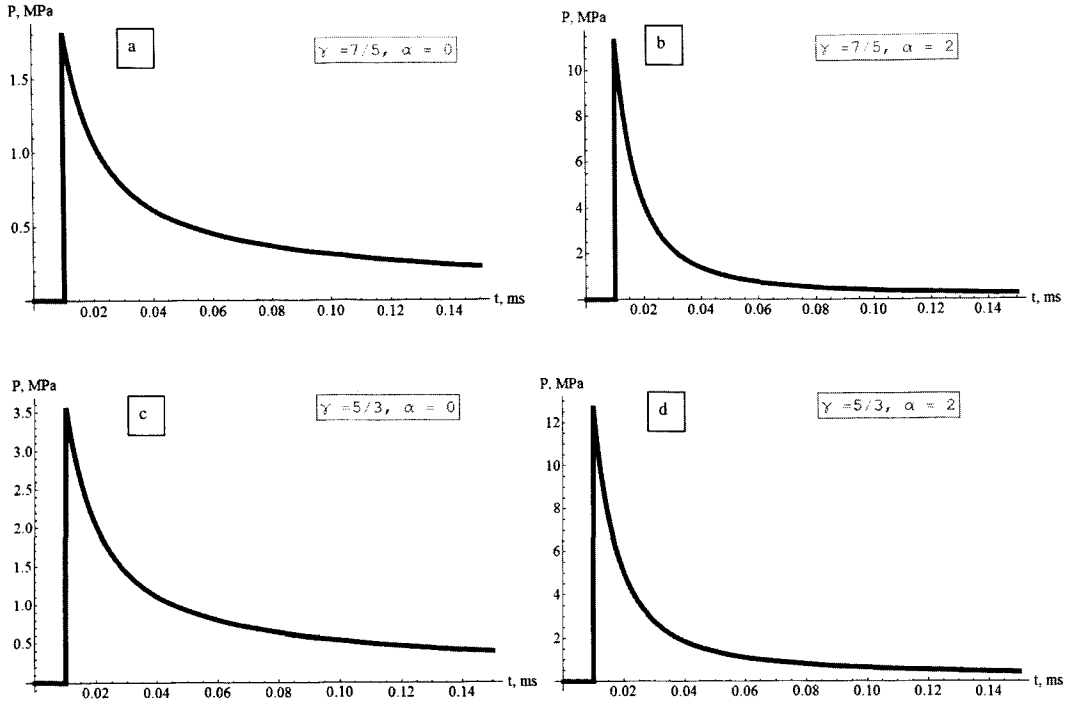

FIG. 3. Results of modeling of the force per unit area, including gas pressure and the contribution of the drag. Explosion of 0.5 g of Al/Bi_2O_3 mixture occurs at an end of a cylindrical reactor with the radius 30.7 mm, and is measured by a detector at a distance 115 mm from the explosion. (a) $\gamma = \frac{7}{5}$, $\alpha = 0$; (b) $\gamma = \frac{7}{5}$, $\alpha = 2$; (c) $\gamma = \frac{5}{3}$, $\alpha = 0$; (d) $\gamma = \frac{5}{3}$, $\alpha = 2$.

given in Eq. (A13); $\mathcal{Z}$ is an explicit function of $\mathcal{V}(\xi)$ given in Eq. (A5), and $\mathcal{D}(\xi)$ is defined in Eq. (A14); parameter β can be found from an explicit integral (A17) and is dependent on the gas constant γ. Such an explicit self-similar solution allows us to compute the pressure together with the contribution of the drag force per unit area

$$P + \frac{1}{2}\alpha\rho v^2 = \left(\frac{4L^2\rho_1}{9t^2}\right)\left(\frac{1}{\gamma}\mathcal{D}\mathcal{Z} + \frac{1}{2}\alpha\mathcal{D}\mathcal{V}^2\right),$$
$$\mathcal{V} \equiv \mathcal{V}(\xi[t]), \quad \xi[t] = \left(\frac{\rho_1 L^3 S}{Et^2\beta^3}\right)^{\frac{1}{3}}. \tag{16}$$

III. SIMULATION OF PRESSURE WAVES

A. Numerical simulation of the self-similar solution

The pressure measured by the detector depends on the boundary conditions at the detector. We first discuss the case where one end of a reactor is open, and a flow of gas is incoming onto the detector. In that case, the force per unit area measured by the detector will include a contribution of gas pressure and of drag force of the incoming flow. In the case when the detector is parallel to the flow, the drag coefficient $\alpha = 0$. In the case when the detector is perpendicular to the flow, the drag can be estimated by a drag on a long plate, with $\alpha = 2$ (in our test geometry, the detector significantly disrupts the flow and the drag is high). A semi-analytic numerical simulation of the time dependence of the pressure waves have been conducted by using the self-similar solution described in detail in Sec. II and in the Appendix. Such a simulation is computationally fast and is free from hard to control numerical errors and various uncontrollable extraneous factors that complicate the interpretation of experiments. This simulation should complement the experimental results already available (Figure 1 from Ref. 9).

In Figure 3, we plot the time dependence of the pressure which will be observed at detector and a distance L from the explosion along the reactor axes, in accordance with our self-similar solution, for $\alpha = 0$ and $\alpha = 2$. We note that contribution of the drag is significant, and when the drag is taken into account, the result of computation is in good match with the experiment.

In Figure 4, we plot the experimental results for the peak pressure at the detector times the detector volume, as a function of mass of the explosive Al/Bi_2O_3 mixture in grams.

The theoretical prediction of the peak pressure is a linear dependence on the explosive mass, since according to Eq. (14) the peak pressure is proportional to the total energy released into the gas, which in turn is proportional to the mass of the explosive mixture. We assume that out of the total released energy, 2.12 kJ/g of Al/Bi_2O_3 mixture, a portion of the energy is used up for melting of Al_2O_3 oxide (~20% of the mass, at 1.01 kJ/g), and the rest of the energy is released into the gas. In Figure 4, we plot the theoretical prediction of the peak pressure dependence on the mass of the explosive Al/Bi_2O_3 mixture, taking the drag coefficient $\alpha = 2$.

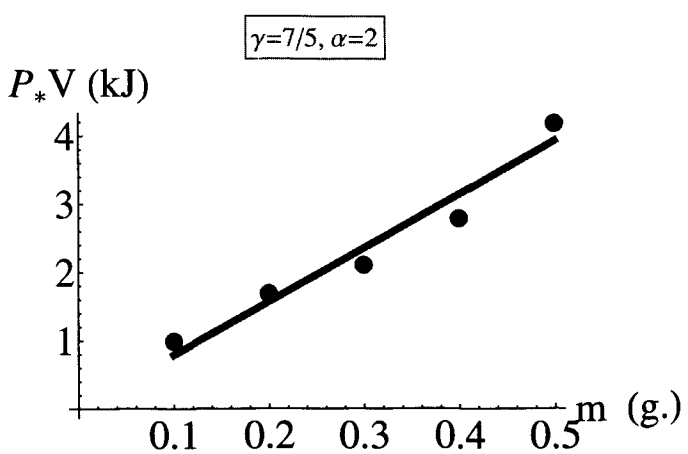

FIG. 4. P_*V dependence on mass of Al/Bi_2O_3 mixture, where P_* is the peak pressure at a detector, and V is the chamber volume. Solid line: the theoretical prediction for $\gamma = \frac{7}{5}$, and the drag coefficient $\alpha = 2$. Dots: the experimental data.

Comparison of the theoretical peak pressure per unit mass, as a function of γ, shown in Figure 5, with the experimental slope suggests that the best match corresponds to $\gamma \sim 1.36$.

B. Peak pressure measured at a closed wall

The case of a flow coming onto a closed wall is more complicated, since reflection of the shock wave needs to be taken into account. An exact analytic solution is unknown in that case; however, an estimate of pressure can be made, based on the knowledge of the pressure in the incoming wave and using Rankine-Hugoniot jump conditions (5)-(8). Such a computation was done by Zel'dovich and Raizer,[19] with the result that the peak pressure measured at the closed wall when the shock wave is reflected back is given by

$$\frac{3\gamma - 1}{\gamma - 1} P_*, \tag{17}$$

where P_* is the incoming shock wave pressure. Taking P_* of the incoming shock wave given by our self-similar solution, for 0.5 g of Al/Bi_2O_3 mixture in $V = 0.342$ L, reactor that yields pressure at a closed wall of 17.75 MPa for $\gamma = \frac{5}{3}$ and 14.6 MPa for $\gamma = \frac{7}{5}$.

C. Comparing gas dynamic and oxidation velocities

We recall that for a self-similar solution, position of a gas dynamic shock is given by

$$X = \beta \left(\frac{Et^2}{S\rho_1}\right)^{\frac{1}{3}},$$

and the gas dynamic velocity of the shock wave is

$$u = \frac{dX}{dt} = \frac{2X}{3t} = \frac{2\beta}{3}\left(\frac{E}{S\rho_1 t}\right)^{\frac{1}{3}},$$

where E is the released energy, S is a cross section area of a reactor, and ρ_1 the initial density (Eqs. (9) and (10)). Here we would like to compare these results with an experiment

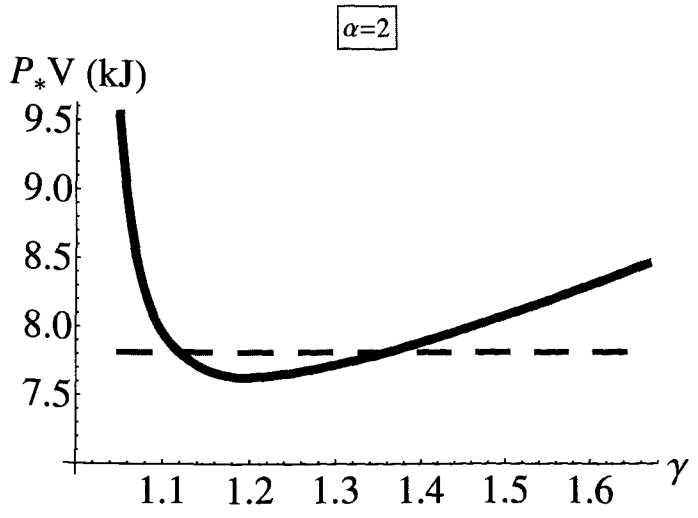

FIG. 5. Solid curve: theoretical P_*V per unit mass of Al/Bi_2O_3 mixture, in kJ/g, as a function of γ. Here P_* is the peak pressure, and V is the chamber volume. The drag coefficient α is taken to be 2. The experimental value of P_*V per unit mass is indicated by a dashed horizontal line.

where a velocity was measured somewhere inside the explosive mixture[11] (and not for a description of gas dynamics, as we do in other sections).

Suppose that a measurement occurs at a distance h from the place where reaction started. The time t can be found from the condition $X = h$, thus

$$t_* = \left(\frac{\rho_1 h^3 S}{\beta^3 E}\right)^{\frac{1}{2}}.$$

For the velocity u this yields

$$u = \frac{2\beta^{\frac{3}{2}}}{3}\left(\frac{E}{hS\rho_1}\right)^{\frac{1}{2}}. \tag{18}$$

To get an estimate for u, it is natural to assume that the released energy is the energy of the explosive mixture behind the shock wave (that is in a cylinder of height h), and that ρ_1 here is the density of the explosive mixture. With this, $hS\rho_1$ is the mass of exploding mixture in a cylinder of height h, and $q_m = \frac{E}{hS\rho_1} = 2.12\text{MJ/kg}$ is the reaction energy release per unit mass. Thus we get an estimate

$$u = \frac{2}{3}\sqrt{\beta^3 q_m}. \tag{19}$$

For $\gamma = \frac{5}{3}$, we have $\beta = 1.49$ (and for smaller γ we have smaller β). Thus taking $\beta = 1.49$, we get the gas dynamic shock wave velocity estimate

$$u \sim 1700\,\text{m/s}. \tag{20}$$

Experimental results for the oxidation velocity in the explosive mixture, measured by times of flashes recorded by detectors, is $v_o \sim 2500\,\text{m/s}$. These results suggest that oxidation velocity is faster than the gas dynamic shock wave velocity, and so our assumption of instantaneous explosion is justified.

ACKNOWLEDGMENTS

The research was sponsored by the Air Force Research Laboratory (AFRL) at the Eglin AFB in Florida under Agreement No. FA8651-12-1 0001 (96ABW-2012-0287). The U.S. Government is authorized to reproduce and distribute reprints for Governmental purposes not withstanding any copyright notation thereon. The views and conclusions contained herein are those of the authors and should not be interpreted as necessarily representing the official policies or endorsements, either expressed or implied, of Air Force Research Laboratory or the U.S. Government.

APPENDIX: DERIVATION OF SELF-SIMILAR SOLUTION

1. A self-similar solution in a cylindrical reactor

A self-similar solution depends on x and t via a dimensionless variable

$$\xi = \frac{x}{X} = \left(\frac{\rho_1 x^3 S}{E t^2 \beta^3}\right)^{\frac{1}{3}}. \tag{A1}$$

We introduce dimensionless variables for the velocity, density, and pressure. Actually, instead of the pressure, it is convenient to introduce a combination $\frac{\gamma P}{\rho}$ denoted by C^2.

$$v = \frac{2x}{3t}\mathcal{V}(\xi), \quad \rho = \rho_1 \mathcal{D}(\xi), \quad \frac{\gamma P}{\rho} = \left(\frac{2x}{3t}\right)^2 \mathcal{Z}(\xi). \tag{A2}$$

Boundary conditions correspond to the shock wave discontinuity $\xi = 1$. It follows from Eqs. (6)–(8) that such boundary conditions are

$$\mathcal{V}(1) = \frac{2}{\gamma+1}, \quad \mathcal{D}(1) = \frac{\gamma+1}{\gamma-1}, \quad \mathcal{Z}(1) = \frac{2\gamma(\gamma-1)}{(\gamma+1)^2}. \tag{A3}$$

We note that for a one dimensional adiabatic flow, energy conservation (2) follows from Eq. (1); moreover, for a flow with nonzero velocity the momentum conservation equation (the first equation in Eq. (1)) may be replaced by the energy conservation (2). We show that in Sec. II of the Appendix.

Substitution of Eq. (A2) into the first gas dynamic equation in Eq. (2) gives

$$\frac{\partial}{\partial t}\left(\rho_1 \mathcal{D}\left(\frac{4x^2}{9t^2}\right)\left(\frac{\mathcal{Z}}{\gamma(\gamma-1)} + \frac{\mathcal{V}}{2}\right)\right) + \frac{\partial}{\partial x}\left(\rho_1 \mathcal{D}\left(\frac{2x}{3t}\mathcal{V}\right)\left(\frac{4x^2}{9t^2}\right)\left(\frac{\mathcal{Z}}{(\gamma-1)} + \frac{\mathcal{V}}{2}\right)\right) = 0.$$

Canceling out the constant factor ρ_1 and using the chain rule and

$$\frac{\partial \xi}{\partial t} = -\frac{2\xi}{3t}, \quad \frac{\partial \xi}{\partial x} = \frac{\xi}{x}, \tag{A4}$$

yields

$$\left(\frac{8x^2}{9t^3}\right)\left\{\frac{1}{3}\frac{\partial}{\partial \ln \xi}\left[\mathcal{D}\left(\left(\frac{\mathcal{V}}{\gamma-1} - \frac{1}{\gamma(\gamma-1)}\right)\mathcal{Z} + (\mathcal{V}-1)\frac{\mathcal{V}^2}{2}\right)\right] - \left[\mathcal{D}\left(\left(\frac{\mathcal{V}}{\gamma-1} - \frac{1}{\gamma(\gamma-1)}\right)\mathcal{Z} + (\mathcal{V}-1)\frac{\mathcal{V}^2}{2}\right)\right]\right\} = 0,$$

here the term with $\frac{\partial}{\partial \ln \xi}$ appears from the differentiation functions of ξ using the chain rule, and the remaining terms appear from the differentiation of the explicit x and t in the coefficients. We can write this equation as

$$\frac{d\mathcal{I}}{d\ln\xi} = -3\mathcal{I}, \quad \mathcal{I} := \mathcal{D}\left\{\frac{\gamma\mathcal{V}-1}{\gamma(\gamma-1)}\mathcal{Z} + \frac{1}{2}(\mathcal{V}-1)\mathcal{V}^2\right\},$$

while the boundary conditions (A3) imply that

$$I|_{\xi=1} = \frac{\gamma+1}{\gamma-1}\left\{\left(\gamma\frac{2}{\gamma+1} - 1\right)\frac{2\gamma(\gamma-1)}{\gamma(\gamma-1)}\frac{2\gamma(\gamma-1)}{(\gamma+1)^2} + \frac{1}{2}\left(\frac{2}{\gamma+1} - 1\right)\left(\frac{2}{\gamma+1}\right)^2\right\} = \frac{\gamma+1}{\gamma-1}\left\{\frac{2(\gamma-1)}{(\gamma+1)^3} - \frac{2(\gamma-1)}{(\gamma+1)^3}\right\} = 0.$$

It than follows that $I(\xi) = 0$ for all ξ. We can use the relation $I(\xi) = 0$ to express $\mathcal{Z}$ as a function of $\mathcal{V}$

$$\mathcal{Z} = \frac{\gamma(\gamma-1)\mathcal{V}^2(\mathcal{V}-1)}{2(\gamma\mathcal{V}-1)}. \tag{A5}$$

For an ideal gas, the second gas dynamic equation in Eq. (1) can be written as

$$\left(\frac{\partial}{\partial t} + v\frac{\partial}{\partial x}\right)\ln\frac{P}{\rho^\gamma} = 0, \quad \gamma = \frac{c_p}{c_v}.$$

Substituting Eq. (A2) and using the chain rule and Eq. (A4) yields

$$\left(\frac{\partial}{\partial t} + v\frac{\partial}{\partial x}\right)\ln\left(\frac{\rho_1 \mathcal{D}\left(\frac{4x^2}{9t^2}\right)\mathcal{Z}}{\gamma\rho_1\mathcal{D}^\gamma}\right) = \frac{2}{3t}\left\{(\mathcal{V}-1)\left[\frac{\partial \ln \mathcal{Z}}{\partial \ln \xi} + (1-\gamma)\frac{\partial \ln \mathcal{D}}{\partial \ln \xi}\right] + (2\mathcal{V}-3)\right\} = 0, \tag{A6}$$

where the last term is due to differentiation of explicit x, t in the coefficient. Similarly, the last gas dynamic equation (1) give

$$\frac{\partial}{\partial t}(\rho_1\mathcal{D}) + \frac{\partial}{\partial x}\left(\rho_1\mathcal{D}\left(\frac{2x}{3t}\mathcal{V}\right)\right) = \frac{2\rho_1}{3t}\mathcal{D}\left\{\frac{\partial \mathcal{V}}{\partial \ln \xi} + (\mathcal{V}-1)\frac{\partial \ln \mathcal{D}}{\partial \ln \xi} + \mathcal{V}\right\} = 0. \tag{A7}$$

the last term is due to differentiation of explicit x in the coefficient. Equations (A6) and (A7) can be written as

$$\begin{aligned} &\frac{d\mathcal{V}}{d\ln\xi} + (\mathcal{V}-1)\frac{d\ln\mathcal{D}}{d\ln\xi} = -\mathcal{V}, \\ &\frac{d\ln\mathcal{Z}}{d\ln\xi} + (1-\gamma)\frac{d\ln\mathcal{D}}{d\ln\xi} = -\frac{2\mathcal{V}-3}{\mathcal{V}-1}. \end{aligned} \tag{A8}$$

Using Eq. (A5), we have that $\frac{d\ln\mathcal{Z}}{d\ln\xi} = \left(-\frac{1}{1-\mathcal{V}} + \frac{2}{\mathcal{V}} - \frac{\gamma}{\gamma\mathcal{V}-1}\right)\frac{d\mathcal{V}}{d\ln\xi}$. and thus Eq. (A8) can be written in the matrix form as

$$\begin{pmatrix} 1 & -1+\mathcal{V} \\ -\frac{1}{1-\mathcal{V}} + \frac{2}{\mathcal{V}} - \frac{\gamma}{\gamma\mathcal{V}-1} & 1-\gamma \end{pmatrix}\begin{pmatrix} \frac{d\mathcal{V}}{d\ln\xi} \\ \frac{d\ln\mathcal{D}}{d\ln\xi} \end{pmatrix} = \begin{pmatrix} -\mathcal{V} \\ -\frac{3-2\mathcal{V}}{1-\mathcal{V}} \end{pmatrix}. \tag{A9}$$

Solving the linear system (A9) for the derivatives $\frac{d\mathcal{V}}{d\ln\xi}, \frac{d\ln\mathcal{D}}{d\ln\xi}$ we obtain

$$\begin{pmatrix} \frac{d\mathcal{V}}{d\ln\xi} \\ \frac{d\ln\mathcal{D}}{d\ln\xi} \end{pmatrix} = \begin{pmatrix} \frac{-\mathcal{V}(\gamma\mathcal{V}-1)((1+\gamma)\mathcal{V}-3)}{\gamma(1+\gamma)\mathcal{V}^2-2(1+\gamma)\mathcal{V}+2} \\ \frac{\mathcal{V}((2\gamma-1)\mathcal{V}-1)}{(1-\mathcal{V})(\gamma(1+\gamma)\mathcal{V}^2-2(1+\gamma)\mathcal{V}+2)} \end{pmatrix}. \tag{A10}$$

It follows that

$$\frac{d\ln\xi}{d\mathcal{V}} = -\frac{\gamma(1+\gamma)\mathcal{V}^2-2(1+\gamma)\mathcal{V}+2}{\mathcal{V}(\gamma\mathcal{V}-1)((1+\gamma)\mathcal{V}-3)},$$
$$\frac{d\ln\mathcal{D}}{d\mathcal{V}} = \frac{\frac{d\ln\mathcal{D}}{d\ln\xi}}{\frac{d\mathcal{V}}{d\ln\xi}} = -\frac{((2\gamma-1)\mathcal{V}-1)}{(1-\mathcal{V})(\gamma\mathcal{V}-1)((1+\gamma)\mathcal{V}-3))}. \tag{A11}$$

Equation (A11) are easily integrated using partial fractions decomposition

$$\begin{aligned} \frac{d\ln\xi}{d\mathcal{V}} &= \frac{1}{3}\left(-\frac{2}{\mathcal{V}}+\frac{3(\gamma-1)}{(2\gamma-1)}\frac{\gamma}{(\gamma\mathcal{V}-1)}\right. \\ &\quad \left.-\frac{(\gamma+1)(5\gamma-4)}{(2\gamma-1)}\frac{1}{(-3+(1+\gamma)\mathcal{V})}\right), \\ \frac{d\ln\mathcal{D}}{d\mathcal{V}} &= -\frac{2}{(2-\gamma)}\frac{1}{(-1+\mathcal{V})}+\frac{1}{(2\gamma-1)}\frac{\gamma}{(-1+\gamma\mathcal{V})} \\ &\quad -\frac{(1+\gamma)(5\gamma-4)}{(\gamma-2)(2\gamma-1)}\frac{1}{(-3+(1+\gamma)\mathcal{V})}. \end{aligned} \tag{A12}$$

Integrating those equations, with the boundary conditions (A3), yields

$$\xi^3 = \frac{4\left(\frac{\gamma+1}{\gamma-1}(\gamma\mathcal{V}-1)\right)^{\frac{3(\gamma-1)}{2\gamma-1}}(3-(1+\gamma)\mathcal{V})^{-\frac{5\gamma-4}{2\gamma-1}}}{(1+\gamma)^2\mathcal{V}^2}, \tag{A13}$$

$$\mathcal{D} = \frac{\gamma+1}{\gamma-1}\left(\frac{\gamma+1}{\gamma-1}(1-\mathcal{V})\right)^{-\frac{2}{2-\gamma}}\left(\frac{\gamma+1}{\gamma-1}(\gamma\mathcal{V}-1)\right)^{\frac{1}{2\gamma-1}} \times (3-(1+\gamma)\mathcal{V})^{\frac{-(5\gamma-4)}{(\gamma-2)(2\gamma-1)}}. \tag{A14}$$

To find the parameter β in Eq. (9), we require that the total energy of gas equals energy released in the explosion. Since $E = S\int_0^X \rho\left(\frac{v^2}{2}+\frac{c^2}{\gamma(\gamma-1)}\right)dx$, by passing to the dimensionless variables (A2) and (A13) we arrive at

$$E = \frac{4}{9}E\beta^3\int_{\xi=0}^{\xi=1}\mathcal{D}\left(\frac{\mathcal{V}^2}{2}+\frac{\mathcal{Z}}{\gamma(\gamma-1)}\right)\xi^3 d\ln\xi. \tag{A15}$$

Canceling E and changing integration variable to $\mathcal{V}$ we obtain

$$1 = \frac{4}{9}\beta^3\int_{\frac{1}{\gamma}}^{\frac{2}{\gamma+1}}\mathcal{D}\left(\frac{\mathcal{V}^2}{2}+\frac{\mathcal{Z}}{\gamma(\gamma-1)}\right)\xi^3\left(\frac{d\ln\xi}{d\mathcal{V}}\right)d\mathcal{V}, \tag{A16}$$

were ξ is a monotonic function of $\mathcal{V}$; at the lower integration limit, $\mathcal{V}=\frac{1}{\gamma}$ and $\xi=0$; at the upper limit, $\mathcal{V}=\frac{2}{\gamma+1}$ and $\xi=1$. Using Eqs. (A12)–(A14), the integrand can be expressed as an explicit function of $\mathcal{V}$, which allows us to compute β, in terms of an explicit integral over $\mathcal{V}$

$$\begin{aligned} \beta^3 &= \frac{9}{8}(\gamma-1)^{\frac{3\gamma^2-4\gamma+2}{2\gamma^2-5\gamma+2}}(1+\gamma)^{-\frac{\gamma(1+\gamma)}{2\gamma^2-5\gamma+2}} \\ &\quad \times\left(\int_{\frac{1}{\gamma}}^{\frac{2}{\gamma+1}}(1-\mathcal{V})^{-\frac{2}{2-\gamma}}(\gamma\mathcal{V}-1)^{-\frac{\gamma}{2\gamma-1}}(3-(1+\gamma)\mathcal{V})^{\frac{7\gamma^2-14\gamma+6}{(2-\gamma)(2\gamma-1)}}\right. \\ &\quad \left.\times\left(\gamma(1+\gamma)\mathcal{V}^2-2(1+\gamma)\mathcal{V}+2\right)d\mathcal{V}\right)^{-1}. \end{aligned} \tag{A17}$$

In particular, a numerical evaluation of the integral in Eq. (A17) yields

$$\beta = \begin{cases} 1.229, & \gamma=\frac{7}{5}, \\ 1.491, & \gamma=\frac{3}{2}. \end{cases} \tag{A18}$$

2. Energy vs. momentum conservation

Let us start with the conservation of energy, entropy, and mass equations

$$\begin{aligned} &\frac{\partial\left(\rho\left(\varepsilon+\frac{v^2}{2}\right)\right)}{\partial t} = -\frac{\partial\left(\rho v\left(\varepsilon+\frac{P}{\rho}+\frac{v^2}{2}\right)\right)}{\partial x} \\ &\qquad \text{(energy conservation)}, \\ &\left(\frac{\partial}{\partial t}+v\frac{\partial}{\partial x}\right)s = 0 \text{ (entropy conservation)}, \\ &\frac{\partial\rho}{\partial t}+\frac{\partial(\rho v)}{\partial x} = 0 \text{ (mass conservation)}. \end{aligned} \tag{A19}$$

We will show that in the one-dimensional case, whenever $v \neq 0$, the momentum conservation follows from Eq. (A19). Indeed, differentiation of the terms in the first equation in Eq. (A19) and grouping them together yields

$$\begin{aligned} &\left(\varepsilon+\frac{v^2}{2}\right)\overbrace{(\partial_t\rho+\partial_x(\rho v))}^{0}+\frac{P}{\rho}\partial_x(\rho v) \\ &\quad +\rho(\partial_t\varepsilon+v\partial_x\varepsilon) \\ &\quad +\rho\left(\partial_t\left(\frac{v^2}{2}\right)+v\partial_x\left(\frac{v^2}{2}\right)\right)+\rho v\partial_x\left(\frac{P}{\rho}\right) = 0, \end{aligned} \tag{A20}$$

here the first line comes from differentiation of ρ with respect to t, or (ρv) with respect to x, while all the other terms are collected in the next 2 lines. Using conservation of mass, given by the last equation in Eq. (A19), a term in Eq. (A20) marked by a brace equals zero.

If the entropy is conserved, it follows that for the energy per unit mass ε we have

$$\frac{d\varepsilon}{dt} \equiv \partial_t\varepsilon+v\partial_x\varepsilon = \frac{P}{\rho^2}(\partial_t\rho+v\partial_x\rho).$$

Using this in the second line of Eq. (A20), Eq. (A20) then becomes

$$\frac{P}{\rho}\partial_x(\rho v) + \rho\frac{P}{\rho^2}(\partial_t\rho + v\partial_x\rho) + \\ + \rho v(\partial_t v + v\partial_x v) + \rho v\partial_x\left(\frac{P}{\rho}\right) = 0, \quad \text{(A21)}$$

the last line in Eq. (A21) comes from the last line in Eq. (A20), and all other surviving terms are written in the first line. Expanding the second term on the first line of Eq. (A21) and combining with the first term on that line, we get

$$\frac{P}{\rho}\overbrace{(\partial_t\rho + \partial_x(\rho v))}^{0} + \rho v\frac{P}{\rho^2}\partial_x\rho \\ + \rho v(\partial_t v + v\partial_x v) + \rho v\partial_x\left(\frac{P}{\rho}\right) = 0.$$

The surviving term on the first line and the last term in the second line combine together into $\rho v\frac{1}{\rho}\partial_x P$, thus factoring out ρv we get

$$\rho v\left(\partial_t v + v\partial_x v + \frac{1}{\rho}\partial_x P\right) = 0.$$

The term in the brackets must vanish (but we need to use $v \neq 0$ to claim that), giving rise to the Euler equation

$$\rho(\partial_t v + v\partial_x v) = -\partial_x P.$$

Let us add a term $v(\partial_t\rho + \partial_x(\rho v))$, which equals zero due to the mass conservation. Grouping terms, we arrive at Eq. (A22), the momentum conservation

$$\rho\partial_t v + \rho v\partial_x v + v\partial_t\rho + v\partial_x(\rho v) = -\partial_x P,$$

thus

$$\partial_t(\rho v) = -\partial_x(\rho v^2 + P). \quad \text{(A22)}$$

We note that for a self-similar solution, $v > 0$ for $x > 0$; at $x = 0$ momentum conservation (A22) is easily verified directly. Indeed, using Eq. (A2) both sides of Eq. (A22) equal zero.

Using the same reasoning but in reverse order, conservation of energy can be shown to follow from gas dynamic equation (1).

[1]D. D. Dlott, "Thinking big (and small) about energetic materials," Mater. Sci. Technol. **22**(4), 463 (2006).
[2]E. L. Dreizin, "Metal-based reactive nanomaterials," Prog. Energy Combus. Sci. **35**, 141–167 (2009).
[3]K. S. Martirosyan, "Nanoenergetic gas generators: Principles and applications," J. Mater. Chem. **21**, 9400–9405 (2011).
[4]K. S. Martirosyan, L. Wang, and D. Luss, "Novel nanoenergetic system based on iodine pentoxide," Chem. Phys. Lett. **483**, 107 (2009).
[5]V. E. Sanders, B. W. Asay, T. J. Foley, B. C. Tappan, A. N. Pacheco, and S. F. Son, "Reaction propagation of four nanoscale energetic composites (Al-MoO_3, Al-WO_3, Al-CuO, and Bi_2O_3)," J. Propul. Power **23**(4), 707–714 (2007).
[6]J. A. Puszynski, C. J. Bulian, and J. J. Swiatkiewicz, "Processing and ignition characteristics of aluminum-bismuth trioxide nanothermite system," J. Propul. Power **23**, 698 (2007).
[7]W. L. Perry, B. C. Tappan, B. L. Reardon, V. E. Sanders, and S. F. Son, "Energy release characteristics of the nanoscale aluminum-tungsten oxide hydrate metastable intermolecular composite," J. Appl. Phys. **101**(6), 064313/1–064313/5 (2007).
[8]S. H. Kim and M. R. Zachariah, Adv. Mater. **16**, 1821 (2004).
[9]L. Wang, D. Luss, and K. S. Martirosyan, "The behavior of nanothermite reaction based on Bi_2O_3/Al," J. Appl. Phys. **110**, 074311 (2011).
[10]K. S. Martirosyan, L. Wang, A. Vicent, and D. Luss, "Synthesis and performance of bismuth trioxide nanoparticles for high energy gas generator use," Nanotechnology **20**, 405609 (2009).
[11]K. S. Martirosyan, L. Wang, A. Vicent, and D. Luss, "Nanoenergetic gas-generator: Design and performance," Propellants, Explos., Pyrotech. **34**, 532 (2009).
[12]J. von Neumann, "The point source solution," *Collected Works* (Permagon, 1963), Vol. 6, p. 219.
[13]G. I. Taylor, "The formation of a blast wave by a very intense explosion. II. The atomic explosion of 1945," Proc. R. Soc. A **201**, 159–186 (1950).
[14]L. I. Sedov, Dokl. Akad. Nauk SSSR **52**, 7–20 (1946); L. I. Sedov, *Similarity and Dimensional Methods in Mechanics*, 6th ed. (Nauka, Moscow, 1967), p. 428.
[15]L. D. Landau and E. M. Lifshitz, *Fluid Mechanics*, 2nd ed. (Reed Publishing, 1987), Vol. 6.
[16]G. K. Batchelor, *Fluid Dynamics* (Cambridge University Press, 2000).
[17]W. P. Graebel, *Engineering Fluid Mechanics* (Taylor & Francis, 2001).
[18]G. Szuladzinski, *Formulas for Mechanical and Structural Shock and Impact* (CRC, 2009).
[19]Ya. B. Zel'dovich and Yu. P. Raizer, *Physics of Shock Waves and High-Temperature Hydrodynamic Phenomena* (Dover Publications, 2002).